

Reorientation-effect measurement of the first 2^+ state in ^{12}C : confirmation of oblate deformation

M. Kumar Raju^{a,b}, J. N. Orce^{a,*}, P. Navrátil^c, G. C. Ball^c, T. E. Drake^d, S. Triambak^{a,b}, G. Hackman^c, C. J. Pearson^c, K. J. Abrahams^a, E. H. Akakpo^a, H. Al Falou^c, R. Churchman^c, D. S. Cross^e, M. K. Djongolov^c, N. Erasmus^a, P. Finlay^f, A. B. Garnsworthy^c, P. E. Garrett^f, D. G. Jenkins^g, R. Kshetri^c, K. G. Leach^f, S. Masango^a, D. L. Mavela^a, C. V. Mehl^a, M. J. Mokgolobotho^a, C. Ngwetsheni^a, G. G. O'Neill^a, E. T. Rand^f, S. K. L. Sjue^c, C. S. Sumithrarachchi^f, C. E. Svensson^f, E. R. Tardiff^c, S. J. Williams^c, J. Wong^c

^aDepartment of Physics & Astronomy, University of the Western Cape, Bellville-7535, South Africa

^bThemba LABS, National Research Foundation, PO Box 722, 7129 Somerset West, South Africa

^cTRIUMF, 4004 Wesbrook Mall, Vancouver, British Columbia V6T 2A3, Canada

^dDepartment of Physics, University of Toronto, Toronto, Ontario M5S 1A7, Canada

^eDepartment of Chemistry, Simon Fraser University, British Columbia V5A 1S6, Canada

^fDepartment of Physics, University of Guelph, Guelph, Ontario N1G 2W1, Canada

^gDepartment of Physics, University of York, York YO10 5DD, United Kingdom

Abstract

A Coulomb-excitation reorientation-effect measurement using the TIGRESS γ -ray spectrometer at the TRIUMF/ISAC II facility has permitted the determination of the $\langle 2_1^+ || \hat{E}2 || 2_1^+ \rangle$ diagonal matrix element in ^{12}C from particle- γ coincidence data and state-of-the-art no-core shell model calculations of the nuclear polarizability. The nuclear polarizability for the ground and first-excited (2_1^+) states in ^{12}C have been calculated using chiral NN $N^4\text{LO500}$ and NN+3NF350 interactions, which show convergence and agreement with photo-absorption cross-section data. Predictions show a change in the nuclear polarizability with a substantial increase between the ground state and first excited 2_1^+ state at 4.439 MeV. The polarizability of the 2_1^+ state is introduced into the current and previous Coulomb-excitation reorientation-effect analyses of ^{12}C . Spectroscopic quadrupole moments of $Q_s(2_1^+) = +0.053(44)$ eb and $Q_s(2_1^+) = +0.08(3)$ eb are determined, respectively, yielding a weighted average of $Q_s(2_1^+) = +0.071(25)$ eb, in agreement with recent *ab initio* calculations. The present measurement confirms that the 2_1^+ state of ^{12}C is oblate and emphasizes the important role played by the nuclear polarizability in Coulomb-excitation studies of light nuclei.

Keywords: Reorientation effect, Spectroscopic quadrupole moment, *ab initio* calculations, nuclear polarizability

Electric quadrupole matrix elements are key quantities in probing the collective structure of nuclei as they are a sensitive and direct measure of the quadrupole deformation. The precise determination of these matrix elements reveals the nuclear collectivity caused by the coherent motion of nucleons, and the associated nuclear wavefunctions. Modern nuclear theory is providing refined calculations of electric quadrupole matrix elements and related properties in light nuclei. Of particular interest is the testing-ground nucleus ^{12}C , as this is computationally accessible to most modern theoretical approaches, including *ab initio* [1–9] and cluster

calculations [10–15]. Cluster calculations in ^{12}C suggest that the admixture of α -cluster wavefunctions may have a pronounced effect on the shape of mean-field states at lower energies. Considerable α -cluster triangle admixtures of 52% and 67% for the ground and 2_1^+ states, respectively, are predicted by fermionic molecular dynamics (FMD) calculations [12], whereas a mean-field contribution of 15% is predicted for the 0_2^+ Hoyle state [16]; the state crucial to fusion of three α particles in the core of massive stars. Moreover, cluster models predict a combination of triangular oblate shapes for the ground state and first 2_1^+ excitation in ^{12}C [10–12]. Mean-field calculations using a relativistic energy-density functional also show a cluster-like structure for the ground state of ^{20}Ne [17].

*Corresponding author

Email addresses: jnorce@uwc.ac.za (J. N. Orce),

Deceased. (R. Churchman)

Experimentally, this strong mixing between the 0_2^+ Hoyle and 0_1^+ ground states is supported by the largest known electric monopole transition strength, $10^3 \times \rho^2(E0) = 500(81)$, determined from electron scattering measurements [18], which corresponds to about a 30% increase in the mean squared charge radius for the Hoyle state.

The spectroscopic quadrupole moment, $Q_s(J)$, provides a measure of the extent to which the nuclear charge distribution in the laboratory frame acquires an ellipsoidal shape [19, 20], and can be determined for states with angular momentum $J \neq 0, \frac{1}{2}$ [21]. For the 2_1^+ state, assuming an ideal rotor, $Q_s(2_1^+)$ is related to the intrinsic quadrupole moment, Q_0 , in the body-fixed frame by $Q_s(2_1^+) = -\frac{2}{7} Q_0$ [21]. Most theoretical approaches predict a very similar $Q_s(2_1^+) \approx +0.06$ eb for ^{12}C [1, 6, 7, 22–24], which supports a substantial oblate deformation. Recent *ab initio* calculations [1, 6, 7] provide theoretical uncertainties in their results which makes for more meaningful comparison with experiment. Among those worth noting are no-core shell model (NCSM) calculations of $Q_s(2_1^+)$ values with unprecedented high precision [3, 6, 7].

The reorientation effect [19, 20, 25] (RE) in Coulomb excitation measurements at energies well below the Coulomb barrier – so-called safe Coulomb excitation – provides a powerful spectroscopic probe for extracting $\langle 2_1^+ || \hat{E}2 || 2_1^+ \rangle$ diagonal matrix elements, which can be directly related to the $Q_s(2_1^+)$ value as $Q_s(2_1^+) = 0.75793 \langle 2_1^+ || \hat{E}2 || 2_1^+ \rangle$ [25].

The only RE measurement of the 2_1^+ state at 4.439 MeV in ^{12}C was performed at safe energies by Vermeer *et al.* [26] through a measurement of inelastically scattered ^{12}C ions by a ^{208}Pb target. The scattered ^{12}C ions were momentum analyzed using a magnetic spectrometer and detected at the focal plane using a position sensitive multi-wire proportional counter placed at a scattering angle in the laboratory frame of $\theta = 90^\circ$. A value of $Q_s(2_1^+) = +0.06(3)$ eb was determined using the nominal nuclear polarizability parameter $\kappa(g.s.) = 1$ determined for the ground state of heavier nuclei [27]. This parameter represents the ratio of the observed isovector giant-dipole-resonance (GDR) effect to that predicted by the hydrodynamic model [27], and is a pivotal ingredient in the RE analysis of light nuclei, where $\kappa > 1$ values are generally observed [26–34].

In this work, we perform a safe Coulomb-excitation RE study of the high-lying 2_1^+ state in ^{12}C using particle– γ coincidence measurements and state-of-the-art NCSM calculations of the nuclear polarizabilities $\kappa(g.s.)$ and $\kappa(2_1^+)$. Although there seems to be a good agreement between previous theoretical and ex-

perimental values of $Q_s(2_1^+)$, the present result emphasizes the crucial importance of determining κ in Coulomb-excitation studies of loosely-bound light nuclei. The main advantage of the particle– γ coincidence technique lies in the absence of target contaminants in the Doppler-corrected γ -ray spectrum.

For this measurement, a beam of $^{12}\text{C}^{3+}$ ions, delivered to the TRIUMF/ISAC II facility [35] at 4.975 AMeV, has been used to populate the 2_1^+ state at 4.439 MeV in ^{12}C through Coulomb excitation. The beam energy was chosen in conformity with Spear’s prescription of a minimum separation between nuclear surfaces of $S(\vartheta)_{min} \gtrsim 6.5$ fm [36] to avoid Coulomb-nuclear interferences, where ϑ is the scattering angle in the center-of-mass frame. An average intensity of $\approx 5 \times 10^8$ particles/s was delivered to the TIGRESS array [37] over approximately three days, and impinged on a 3 mg/cm² thick ^{194}Pt target (96.45% enriched). The online data were collected in event-by-event mode using a high-speed digital data acquisition system with 100 MHz TIG-10 digital electronics modules.

The γ rays de-exciting the beam and target nuclei were detected using eight TIGRESS HPGe clover detectors positioned at 14.5 cm from the target, and covering around 15% of 4π . The scattered ions and recoiling particles were detected in a double-sided, CD-type silicon detector (S2 type from Micron Semiconductors [38]), which was mounted 19.4 mm downstream. The experimental set up is very similar to the one given in Ref. [29] apart from the use of an S2 detector, which is segmented into 48 rings and 16 azimuthal sectors on the ohmic side, and has the 12 outermost rings incomplete; hence, it does not present full azimuthal or ϕ symmetry. The scattered beam was fully stopped in the 500- μm thick S2 detector. Additional experimental details will be presented in a separate manuscript.

The energy calibration and relative photo-peak efficiency ε of the TIGRESS detectors were determined using standard radioactive ^{152}Eu and ^{56}Co sources. The calibration of all the silicon strips was done using a triple α source containing ^{239}Pu , ^{241}Am and ^{244}Cm , together with higher-energy calibration points provided by the elastically scattered beam particles simulated with GEANT4 [39], both including energy losses [40] in the ^{194}Pt target and the 0.58-mg/cm² thick aluminum coating on the ohmic side of the S2 detector facing the scattered ^{12}C beam. Typical particle-energy spectra for the innermost (a) and outermost (b) rings at average angles of $\theta = 31.7^\circ$ and 60.7° are shown in Fig. 1.

Particle– γ coincidence events were selected by employing the condition that each hit in a TIGRESS detector has a hit in both a ring (θ) and a sector (ϕ) of the

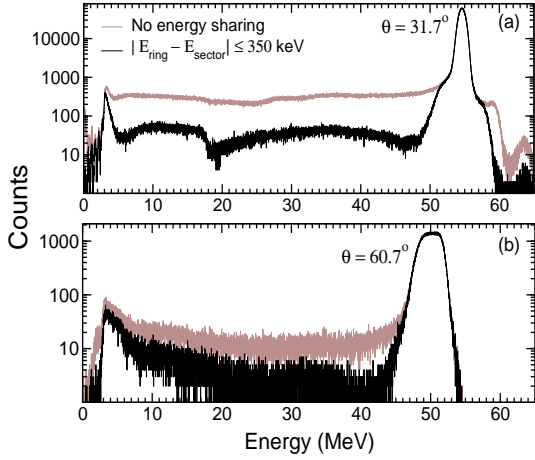


Figure 1: Typical particle-energy spectra for the rings at average θ angles of (a) 31.7° and (b) 60.7° obtained with (black) and without (light brown) an energy-sharing condition, see text for details.

S2 detector within a coincidence time window of approximately 195 ns. The corresponding γ -ray spectra were further cleaned by subtracting random coincidence events outside the 195-ns time window. An additional energy-sharing condition of $|E_{ring} - E_{sector}| \leq 350$ keV between each ring and sector yields a large background reduction in the particle spectra and enables a better selection of the inelastic peaks [29]. This energy-sharing condition was chosen to achieve the most optimum background reduction while conserving the area of the 4439-keV peak in the γ -ray spectrum. Figure 1 illustrates the effect with a large background reduction (black), as compared with no energy-sharing condition (brown), at low and intermediate energies. Finally, inelastic particle gates can be set on each ring particle spectrum to collect solely Coulomb-excitation events in coincidence with the γ ray of interest.

Figure 2 shows the Doppler-corrected γ -ray energy spectrum obtained from the TIGRESS array after applying particle and time tagging conditions. The spectrum shows the 328- and 4439-keV γ -ray transitions depopulating the 2_1^+ level in ^{194}Pt and ^{12}C , respectively.

Another second-order effect in Coulomb-excitation perturbation theory which may influence, particularly for light nuclei [26, 28, 29], the determination of both the sign and magnitude of $\langle 2_1^+ || E2 || 2_1^+ \rangle$ is the $E1$ polarizability [41]. This involves virtual electric-dipole excitations via the GDR that polarize the shape of the 2_1^+ state through two-step processes of the type $0_1^+ \rightarrow 1_{GDR}^- \rightarrow 2_1^+$. In particular, light nuclei present typical values of $\kappa > 1$ [28], which has a net effect of shift-

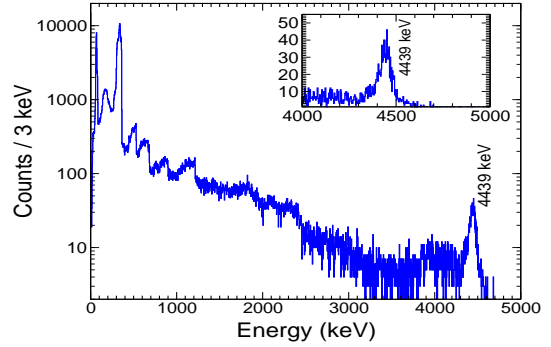


Figure 2: Doppler-corrected γ -ray energy spectrum generated by employing particle- γ , time, energy-sharing and inelastic-particle coincidence conditions.

ing the measured $Q_S(2_1^+)$ values towards more prolate shapes.

The polarization potential V_{pol} generated by the $E1$ polarizability is incorporated into Coulomb-excitation analyses by a reduction in the quadrupole interaction, $V_0(t)$, which results in an effective potential, $V_{eff}(t)$ [30],

$$\begin{aligned} V_{eff}(t) &= V_0(t) (1 - V_{pol}(t)) \\ &= V_0(t) \left(1 - z \frac{a}{r(t)}\right), \end{aligned} \quad (1)$$

where a is the half-distance of closest approach in a head-on collision and $r(t)$ the magnitude of the projectile-target position vector. For the case of projectile excitation, z is given by [25],

$$z = \frac{10Z_t \alpha}{3Z_p R^2 a} \approx 0.0039 \kappa \frac{T_p A_p}{Z_p^2 (1 + A_p/A_t)}, \quad (2)$$

with $R = 1.2A^{1/3}$ fm being the nuclear radius, T_p the kinetic energy (in MeV) in the laboratory frame, $\alpha = \frac{\hbar c}{2\pi^2} \sigma_{-2}$ the nuclear polarizability, where $\alpha = 2P_0$ as defined by Alder and Winther [25], and κ the polarizability parameter. The (-2) moment of the total photoabsorption cross section, σ_{-2} , and κ are related by [28],

$$\sigma_{-2} = 2.4 \kappa A^{5/3} \mu\text{b/MeV}. \quad (3)$$

The value of κ can accordingly be modified in modern Coulomb-excitation codes such as GOSIA [42]. For light nuclei, values of $\kappa > 1$ have been determined by Coulomb-excitation measurements for a few favorable cases where $Q_S(J) = 0$ [30, 32, 34], i.e., for $J = 1/2$ excited states, and shell-model calculations [22, 43]. For the case of arbitrary spins, Häusser and collaborators developed an expression for κ in terms of $E1$

and $E2$ matrix elements [30], $\kappa = \frac{X}{X_0}$, where $X_0 = 0.0004 \frac{A}{2} \text{ eMeV}^{-1}$ and X is given by,

$$X = \frac{\sum_n W(11J_i J_f, 2J_n) \frac{\langle i | \hat{E}1 | n \rangle \langle n | \hat{E}1 | f \rangle}{E_n - E_i}}{\langle i | \hat{E}2 | f \rangle}, \quad (4)$$

where the sum extends over all intermediate states $|n\rangle$ connecting the initial $|i\rangle$ and final $|f\rangle$ states with $E1$ transitions and $W(11J_i J_f, 2J_n)$ is the Racah W -coefficient [44] with $J_i = 0$, $J_f = 2$ and $J_n = 1$ for the case at hand. It is important to note here that the product of two $\hat{E}1$ operators yields an $\hat{E}2$ operator; hence, some of the isoscalar giant quadrupole resonance strength may :

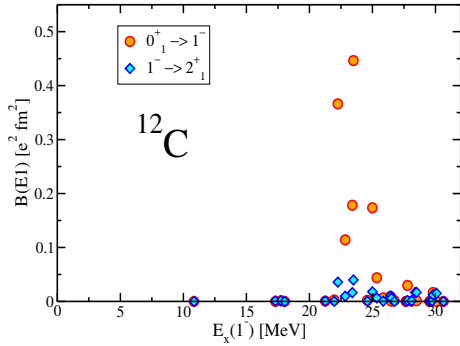


Figure 3: $B(E1)$ strengths calculated with the NCSM using the chiral $NN + 3NF350$ interaction for $0_1^+ \rightarrow 1^-$ and $1^- \rightarrow 2_1^+$ transitions.

In the present work, NCSM calculations have been performed to estimate κ for the ground and 2_1^+ states in ^{12}C . Previous SM calculations of $\kappa(2_1^+) = 0.77$ presumed that all the $E1$ strength from the ground state was concentrated at the GDR energy [22]. Our NCSM calculations used the chiral $NN + 3NF350$ interaction [45–47], including the $N^3\text{LO}$ NN interaction [45] and the local $N^2\text{LO}$ $3N$ interaction [46] with the cutoff of 350 MeV [47], and considered model spaces with basis sizes of $N_{max} = 4$ for the natural and $N_{max} = 5$ for the unnatural parity states. From Eq. 4, which included the $E1$ matrix elements from all the transitions connecting 28 1^- states up to 30 MeV, values of $\kappa(g.s.) = 1.6(2)$ and $\kappa(2_1^+) = 2.2(2)$ are predicted. As shown in Fig. 3, the $E1$ strength is concentrated at an energy of about 24 MeV – the centroid energy of the GDR [48]. The lowest calculated 1^- state energy was set to the lowest found 1^- state at 10.84 MeV. In order to study convergence and determine uncertainties, predictions with the $NN + 3NF350$ interaction have been validated by additional NCSM calculations using the $NN N^4\text{LO500}$ interaction [49, 50] SRG evolved [51] to 2.4 fm^{-1} at the same

$N_{max} = 4/5$ space and at a smaller $N_{max} = 2/3$ space at varied harmonic-oscillator frequencies, as well as at a larger $N_{max} = 6$ space for natural parity and $N_{max} = 7$ for unnatural parity states, which included 22 1^- states up to 30 MeV. The latest calculations yield similar results of $\kappa(g.s.) = 1.5(2)$ and $\kappa(2_1^+) = 2.1(2)$. In general, to improve on the present NCSM description, one should include RGM-like cluster states with explicit α particles, e.g., $^8\text{Be} + \alpha$ and couple them with the currently used NCSM basis. Such approach called NCSM with continuum is now under development. However, the good stability of all the 1^- states with N_{max} demonstrates that our expansion is adequate.

The well-known total photo-absorption cross section measured for the ground state of ^{12}C can be used to benchmark our NCSM calculations. A value of $\sigma_{-2} = 244 \mu\text{b/MeV}$ in the 1985 evaluation by Fuller [52], yields $\kappa(g.s.) = 1.6$ using Eq. 3, in excellent agreement with our NCSM polarizability calculations for the ground state. The consistency of our calculations further supports the value of $\kappa(2_1^+) = 2.2(2)$ implemented in our GOSIA analysis [42] throughout this work.

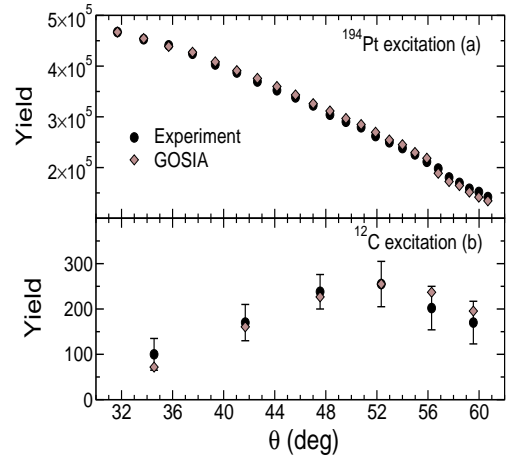


Figure 4: Heavy-ion angular distributions showing experimental and calculated γ -ray yield as a function of laboratory scattering angle, θ , for the de-excitation of the 2_1^+ states in ^{12}C (bottom) and ^{194}Pt (top), see text for details.

The integrated γ -ray yields for the $2_1^+ \rightarrow 0_1^+$ transitions in ^{12}C and ^{194}Pt have been calculated using the semi-classical coupled-channel Coulomb-excitation least-squares code GOSIA [42]. The semi-classical approximation is confirmed from Rutherford scattering cross sections and the calculated Sommerfeld parameter, $\eta = \frac{q}{\lambda} = 31 \gg 1$, where λ is the de Broglie wavelength. Calculations consider the known spectroscopic information such as level lifetimes, branching ratios

and matrix elements, kinematics, detector geometry and beam energy losses. The effect of higher-lying states in ^{12}C has been estimated using GOSIA and considered negligible ($< 0.1\%$). Figure 4 shows the experimental and theoretical heavy-ion angular distributions from the eight clover yields for the $2_1^+ \rightarrow 0_1^+$ transitions in ^{194}Pt (a) and ^{12}C (b). Predictions of the cross sections for populating states in ^{12}C were calculated at fixed values of $\langle 2_1^+ \parallel \hat{E}2 \parallel 0_1^+ \rangle = 0.0630$ eb [53], $\langle 2_1^+ \parallel \hat{E}2 \parallel 2_1^+ \rangle = +0.070$ eb and $\kappa = 2.2$, the intersection point of the centroid of the two bands in Fig. 5, and normalized to the experimental yields with a common normalization factor. The shape of the angular distributions predicted by GOSIA for both ^{194}Pt and ^{12}C are in good agreement with experiment.

The normalization procedure used in Ref. [29] was applied to determine $\langle 2_1^+ \parallel \hat{E}2 \parallel 2_1^+ \rangle$, where Coulomb-excitation curves are determined in the $\langle 2_1^+ \parallel \hat{E}2 \parallel 2_1^+ \rangle - \langle 2_1^+ \parallel \hat{E}2 \parallel 0_1^+ \rangle$ plane by fixing $\langle 2_1^+ \parallel \hat{E}2 \parallel 2_1^+ \rangle$ in steps of 0.01 eb, and varying $\langle 2_1^+ \parallel \hat{E}2 \parallel 0_1^+ \rangle$ until converging with the experimental intensity ratio between target and projectile, I_γ^T/I_γ^P , given by,

$$\frac{\sigma_{E2}^T W(\vartheta)^T}{\sigma_{E2}^P W(\vartheta)^P} = 1.037 \frac{N_\gamma^T \varepsilon_\gamma^P}{N_\gamma^P \varepsilon_\gamma^T} = \frac{I_\gamma^T}{I_\gamma^P}, \quad (5)$$

where $W(\vartheta)$ represents the integrated angular distribution of the de-excited γ rays in coincidence with the inelastic scattered particles [54] and the factor 1.037 accounts for the 96.45% enrichment of the ^{194}Pt target chosen for normalization. The normalization of the γ -ray yield in ^{12}C to the well-known matrix elements in the target nucleus, ^{194}Pt , minimizes systematic effects such as dead time and pile-up rejection. Absolute efficiencies of $\varepsilon_\gamma^P = 0.0162(5)$ and $\varepsilon_\gamma^T = 0.0784(8)$, and total counts of $N_\gamma^P = 1150(40)$ and $N_\gamma^T = 7021190(2650)$ for the 4439- and 328-keV γ -ray transitions, respectively, yield $I_\gamma^T/I_\gamma^P = 1308(62)$. The quoted error on this measurement arises from the uncertainties of N_γ^P (3.5%) and ε_γ^P (3.1%). Other contributions are less significant and include the ϕ asymmetry of the TIGRESS detectors ($< 0.5\%$) [55].

The resulting Coulomb-excitation diagonal band is shown in Fig. 5, where the black dashed line is the central value and the two black solid lines correspond to the 1σ loci limits. The horizontal band represents $\langle 2_1^+ \parallel \hat{E}2 \parallel 0_1^+ \rangle = 0.0630(16)$ eb [53]. Assuming $\kappa(2_1^+) = 2.2$, a positive value of $\langle 2_1^+ \parallel \hat{E}2 \parallel 2_1^+ \rangle = +0.070(71)$ eb is obtained from the intersection of the two bands, corresponding to $Q_s(2_1^+) = +0.053(53)$ eb. The error of $\langle 2_1^+ \parallel \hat{E}2 \parallel 2_1^+ \rangle$ was determined from the overlap

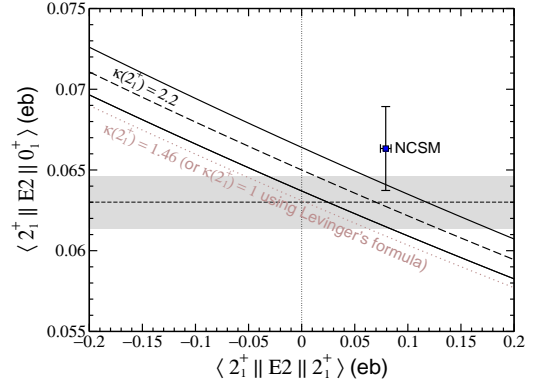


Figure 5: Variation of $\langle 2_1^+ \parallel \hat{E}2 \parallel 0_1^+ \rangle$ as a function of $\langle 2_1^+ \parallel \hat{E}2 \parallel 2_1^+ \rangle$ in ^{12}C for $k(2_1^+) = 2.2$. The horizontal band represents the 1σ boundary for $\langle 2_1^+ \parallel \hat{E}2 \parallel 0_1^+ \rangle = 0.0630(16)$ [53]. For comparison, the square data point shows the result from high-precision NCSM calculations, $Q_s(2_1^+) = +0.060(4)$ eb and $B(E2; 2_1^+ \rightarrow 0_1^+) = 8.8(7)$ e^2fm^4 [6].

region between the two bands assuming central values for the $\langle 2_1^+ \parallel \hat{E}2 \parallel 0_1^+ \rangle$ band, ± 0.045 eb, and the Coulomb-excitation diagonal curve, ± 0.055 eb, added in quadrature. The uncertainty of $\kappa(2_1^+)$, ± 0.01 eb, yield final values of $\langle 2_1^+ \parallel \hat{E}2 \parallel 2_1^+ \rangle = +0.070(72)$ eb and $Q_s(2_1^+) = +0.053(54)$ eb. Moreover, if one uses $\kappa(2_1^+) = 1$ assuming Levinger's formula [27], $\sigma_{-2} = 3.5\kappa A^{5/3} \mu\text{b}/\text{MeV}$ (which corresponds to $\kappa(2_1^+) = 1.46$ using Eq. 3), our data yields $Q_s(2_1^+) = +0.003(54)$ eb, as shown by the dotted brown line in Fig. 5; a value consistent with a spherical shape.

A more precise determination of the statistical uncertainty of $\langle 2_1^+ \parallel \hat{E}2 \parallel 2_1^+ \rangle$ has been done by employing the error minimization procedure in GOSIA [56], considering $\langle 2_1^+ \parallel \hat{E}2 \parallel 0_1^+ \rangle = 0.0630(16)$ eb [53] and $\langle 2_1^+ \parallel \hat{E}2 \parallel 2_1^+ \rangle = 0.070(72)$ eb as initial inputs along with available matrix elements of higher-lying states. Using the six experimental yields given in Fig. 4, the error minimization carried out in a two-step process, by calculating the uncorrelated and correlated errors, yields a final error of $\Delta\langle 2_1^+ \parallel \hat{E}2 \parallel 2_1^+ \rangle = 0.058$ eb, which includes the error of $\kappa(2_1^+)$, ± 0.01 eb. A final value of $Q_s(2_1^+) = +0.053(44)$ eb is determined, which accounts for an additional 5% systematic uncertainty in the GOSIA calculation. The main source of systematic uncertainty is attributed to quantal effects, which are inversely proportional to η [25, 57–59], and could affect the validity of the semi-classical approximation. For $\eta \approx 31$, quantal effects may add an uncertainty of $\leq 3.5\%$ to the present determination of the $Q_s(2_1^+)$ value. If one takes the data from Vermeer

et al. [26] and assumes $\kappa(2_1^+) = 2.2$ and $\langle 2_1^+ || \hat{E}2 || 0_1^+ \rangle = 0.0630(16)$ eb, a potentially more pronounced value of $Q_s(2_1^+) \approx +0.08(3)$ eb is determined, in agreement with the present work. The weighted average of the current and previous work yields a final value of $Q_s(2_1^+) = +0.071(25)$ eb.

The weighted $Q_s(2_1^+)$ value can be compared with state-of-the-art *ab initio* calculations. The high-precision NCSM calculation using the CDB2k NN potential is given in Fig. 5 by the square data point [6], $Q_s(2_1^+) = +0.060(4)$ eb and $B(E2; 2_1^+ \rightarrow 0_1^+) = 8.8(7)$ e²fm⁴. Similar values of $Q_s(2_1^+) = +0.0591(25)$ eb and $Q_s(2_1^+) = +0.059(1)$ eb are calculated, respectively, using chiral NN+3N interactions [7] and the no-core symplectic model [3]. Calculations are in agreement with the weighted average presented in this work.

Unfortunately, the model space that can currently be reached with the NCSM does not allow a calculation of the nuclear polarizability for the 2_2^+ state built on the Hoyle state. One could, however, speculate that if κ further increases with excitation energy, as the nucleus becomes more loosely bound, a more pronounced prolate shape might be expected for the shape of the Hoyle state rotational band. This is in concordance with the prolate bent-arm configuration – with $Q_s(2_2^+) = -0.07(2)$ eb – predicted by *ab initio* calculations using chiral perturbation theory on a lattice [2], and, although with an extremely large prolate deformation, the $Q_s(2_2^+) = -0.21(1)$ eb value predicted by the no-core symplectic model [3]. Such an enhanced polarizability might explain the sudden change in the shape of the Hoyle state, which seems to be in disagreement with early models of cluster formation such as that of Morinaga, where α -cluster structures gradually emerge with increasing excitation energy and are fully realized at the α threshold [60, 61].

In conclusion, the Coulomb-excitation analysis performed in this work using the TIGRESS array and the new value of $\kappa(2_1^+)$ calculated with the NCSM have permitted the determination of the $\langle 2_1^+ || \hat{E}2 || 2_1^+ \rangle$ diagonal matrix element in ¹²C from particle- γ coincidence data. The present work confirms an oblate deformation for the 2_1^+ state in ¹²C, in agreement with recent *ab initio* and cluster-model calculations.

Finally, it is important to emphasize that NCSM calculations show that the polarizability parameter for excited states can be very different from the ground state value determined from total photo-absorption cross-section data. This unanticipated change of the nuclear polarizability from the ground state to the first excitation in ¹²C may not only affect Coulomb-excitation analyses of light nuclei, but in general, as nuclei become less

bound, Coulomb-excitation studies of states at high excitation energies (e.g., superdeformed bands found in nuclei with spherical ground states). This possibility clearly needs further investigations.

Acknowledgements

We thank the accelerator group at TRIUMF for their support during the experiment. This work has been partially supported by the South African National Research Foundation (NRF) under Grants 93500 and the Natural Sciences and Engineering Research Council of Canada. TRIUMF receives federal funding via a contribution agreement through the National Research Council of Canada. JNO thanks J. L. Wood for pointing to the $\hat{E}2$ operator relationship in Eq. 4 and the late D. H. Wilkinson for fruitful discussions. Computing support came from an INCITE Award on the Titan supercomputer of the Oak Ridge Leadership Computing Facility (OLCF) at ORNL, and from Calcul Quebec and Compute Canada.

References

- [1] E. Epelbaum, *et al.*, Phys. Rev. Lett. 106 (2011) 192501.
- [2] E. Epelbaum, *et al.*, Phys. Rev. Lett. 109 (2012) 252501.
- [3] A. C. Dreyfuss, *et al.*, Phys. Lett. B 727 (2013) 511.
- [4] K. Kravvaris, A. Volya, Phys. Rev. Lett. 119 (2017) 062501.
- [5] P. Navrátil, J.P. Vary, B.R. Barrett, Phys. Rev. Lett. 84 (2000) 5728; P. Navrátil, Phys. Rev. C 62 (2000) 054311.
- [6] C. Forssén, R. Roth, P. Navrátil, J. Phys. G 40 (2013) 055105.
- [7] A. Calci, R. Roth, Phys. Rev. C 94 (2016) 014322.
- [8] S.C. Pieper, Nucl. Phys. A 751 (2005) 516c.
- [9] P. Navrátil, W.E. Ormand, Phys. Rev. C 68 (2003) 034305.
- [10] D.J. Marín-Lámbarrí *et al.*, Phys. Rev. Lett. 113 (2014) 012502.
- [11] T. Neff, H. Feldmeier, J. Phys.: Conf. Ser. 569 (2014) 012062.
- [12] M. Chernykh *et al.*, Phys. Rev. Lett. 98 (2007) 032501.
- [13] M. Freer, H.O.U. Fynbo, Prog. Part. Nucl. Phys. 78 (2014) 1.
- [14] Y. Funaki, Phys. Rev. C 92 (2015) 021302(R).
- [15] Y. Yoshida, Y. Kanada-En'yo, Prog. Theor. Exp. Phys. (2016) 123D04.
- [16] F. Hoyle, Astrophys. J. Suppl. Ser. 1 (1954) 121.
- [17] J.-P. Ebran, E. Khan, T. Nikšić and D. Vretenar, Nature 487 (2012) 341.
- [18] T. Kibédi, R.H. Spear, Atom. Data Nucl. Data Tables 89 (2005) 77.
- [19] J. de Boer, J. Eichler, Adv. Nucl. Phys. 1 (1968) 1.
- [20] O. Häusser, Nuclear Spectroscopy and Reactions C, edited by J. Cerny (Academic, New York, 1974).
- [21] A. deShalit, H. Feshbach, Theoretical Nuclear Physics, Volume I: Nuclear Structure, Wiley-Blackwell, 1974.
- [22] F.C. Barker, Aust. J. Phys. 35 (1982) 291.
- [23] Y. Abgrall, B. Morand, E. Caurier, Nucl. Phys. A 192 (1972) 372.
- [24] R.H. Bassel, B.A. Brown, R. Lindsay, N. Rowley, J. Phys. G 8 (1982) 1215.
- [25] K. Alder, A. Winther, Electromagnetic Excitation, North-Holland, Amsterdam, 1975.

- [26] W.J. Vermeer *et al.*, Phys. Lett. B 122 (1983) 23.
- [27] J.S. Levinger, Phys. Rev. 107 (1957) 554.
- [28] J.N. Orce, Phys. Rev. C 91 (2015) 064602.
- [29] J.N. Orce *et al.*, Phys. Rev. C 86 (2012) 041303(R).
- [30] O. Häusser, *et al.*, Nucl. Phys. A 212 (1973) 613.
- [31] E.B. Bazhanov *et al.*, Nucl. Phys. 68 (1965) 191.
- [32] W.J. Vermeer *et al.*, Aust. J. Phys. 37 (1984) 273.
- [33] W.J. Vermeer *et al.*, Aust. J. Phys. 35 (1982) 283.
- [34] J.A. Kuehner *et al.*, Phys. Lett. B 115 (1982) 437.
- [35] J. Dilling, R. Krücken, Hyp. Int. 225 (2014) 111.
- [36] R.H. Spear, Phys. Rep. 73 (1981) 369.
- [37] C.E. Svensson *et al.*, J. Phys. G. 31 (2005) S1663.
- [38] Silicon detectors, <http://79.170.44.80/micronsemiconductor.co.uk/wp-content/uploads/2017/01/cat.pdf>, 2017 (accessed 04.08.17)
- [39] S. Agostinelli *et al.*, Nucl. Instr. Meth. A 506 (2003) 250.
- [40] J.F. Ziegler *et al.*, Nucl. Instr. Meth. B 268 (2010) 1818.
- [41] J. Eichler, Phys. Rev. 133 (1964) B1162.
- [42] T. Czosnyka, D. Cline, C.Y. Wu, Bull. Am. Phys. Soc. 28 (1983) 745.
- [43] F.C. Barker, Aust. J. Phys. 35 (1982) 301.
- [44] G. Racah, Phys. Rev. 62 (1942) 438.
- [45] D.R. Entem, R. Machleidt, Phys. Rev. C 68 (2003) 041001.
- [46] P. Navrátil, Few-Body Syst. 41 (2007) 117.
- [47] R. Roth, A. Calci, J. Langhammer, S. Binder, Phys. Rev. C 90 (2014) 024325.
- [48] S.S. Dietrich and B.L. Berman, Atom. Data Nucl. Data Tables 38 (1988) 199.
- [49] D.R. Entem, N. Kaiser, R. Machleidt, Y. Nosyk, Phys. Rev. C 91 (2015) 014002.
- [50] D.R. Entem, R. Machleidt, and Y. Nosyk, arXiv:1703.05454.
- [51] S.K. Bogner, R.J. Furnstahl, R.J. Perry, Phys. Rev. C 75 (2007) 061001(R).
- [52] E.G. Fuller, Phys. Rep. 127 (1985) 185.
- [53] B. Pritychenko, M. Birch, B. Singh, M. Horoi, Atom. Data Nucl. Data Tables, 107 (2016) 1.
- [54] K. Adler, A. Bohr, T. Huus, B. Mottelson, and A. Winther, Rev. Mod. Phys. 28 (1956) 432.
- [55] M.A. Schumaker *et al.*, Phys. Rev. C 78 (2008) 044321.
- [56] M. Zielińska *et al.*, Eur. Phys. J. A 52 (2016) 99.
- [57] U. Smilansky, Nucl. Phys. A 112 (1968) 185.
- [58] K. Alder and H.K.A. Pauli, Nucl. Phys. A 128 (1969) 193.
- [59] A.E. Kavka *et al.*, Nucl. Phys. A 593 (1995) 177.
- [60] H. Morinaga, Phys. Rev. 101 (1956) 254.
- [61] K. Ikeda, N. Takigawa, H. Horiuchi, Prog. Theor. Phys. Suppl. E68 (1968) 464.